



Research Article

Experimental Analysis of Total Radiated Power by the Open Energy Meter 2G

M. Briccola,¹ P. Giubbini,¹ F. Cascetta,² A. Delle Femine,² D. Gallo,² C. Landi ,² and M. Luiso ²

¹*E-distribuzione S.p.A, Via Ombone 2, 00198 Rome, Italy*

²*Department of Engineering, University of Campania Luigi Vanvitelli, Aversa, CE, Italy*

Correspondence should be addressed to M. Luiso; mario.luiso@unicampania.it

Received 7 February 2019; Revised 16 April 2019; Accepted 7 July 2019; Published 30 September 2019

Academic Editor: Stefano Vitturi

Copyright © 2019 M. Briccola et al. This is an open access article distributed under the Creative Commons Attribution License, which permits unrestricted use, distribution, and reproduction in any medium, provided the original work is properly cited.

The company e-distribuzione S.p.A (the main Italian electricity distributor) has started in 2017 the massive installation of the second-generation smart electrical energy meters. These smart meters have several new features. In particular, the communication functions have been improved to enhance the reliability of the communication towards the concentrator: in addition to the traditional main PLC channel, a radio module has been added with a transmission around the frequency of 169 MHz. This paper assesses the characteristics of the emission due to this radio module, quantifying the total radiated power. The analyses were performed not only inside an anechoic room, to obtain repeatable results, but also in situations close to the normal operating conditions.

1. Introduction

The company e-distribuzione S.p.A. (hereinafter referred to as “ED”) is the main Italian electricity distributor, and it carries out the distribution service in about 7.500 municipalities included in the concession issued by the Ministry of Economic Development in 2003. In these municipalities, ED is also the operator of the measurement activity (Italian Legislative Decree 102/2014), and it is therefore responsible for the installation and maintenance of the meters used to collect the electricity measurement data.

ED has launched the installation of an Advanced Metering Infrastructure (AMI) in 2001, with a project known as Telegestore [1]. This currently working AMI consists of an integrated collection of devices, networks, and computer systems that includes 32 million smart meters at customers’ homes, 380 thousand of data concentrators, and some thousands of meters in medium-voltage/low-voltage (MV/LV) substations fully dedicated to energy service applications (Figure 1). The system is devoted not only to measure and collect electricity metering data, on request or on the basis of

predefined schedule, but it is also able to remotely execute commercial operations like activations, deactivations, contractual power limit changes, and bad payer management.

The basic components of Telegestore are the smart meters (Figure 2(a)) installed on each supply node (point of delivery, POD) that communicate in narrow-band power line communication (PLC) with a concentrator that forwards data to a central database system adopting the GSM/GPRS protocol.

In this context, at the beginning of last autumn, ED has started the massive installation of the second-generation smart meters (Enel Open Meter 2G, Figure 2(b)) that will replace the first generation meters at each POD. The second-generation meter is the result of a process that reflects recent developments in the market and in the technology field of metering and remote management. The innovative features of the new smart meter include the availability of customer consumption data every 15 minutes and a dedicated PLC channel to interact with the customer. With this granular timely picture of the daily energy use, traders can develop tailor-made offers and customers, becoming increasingly

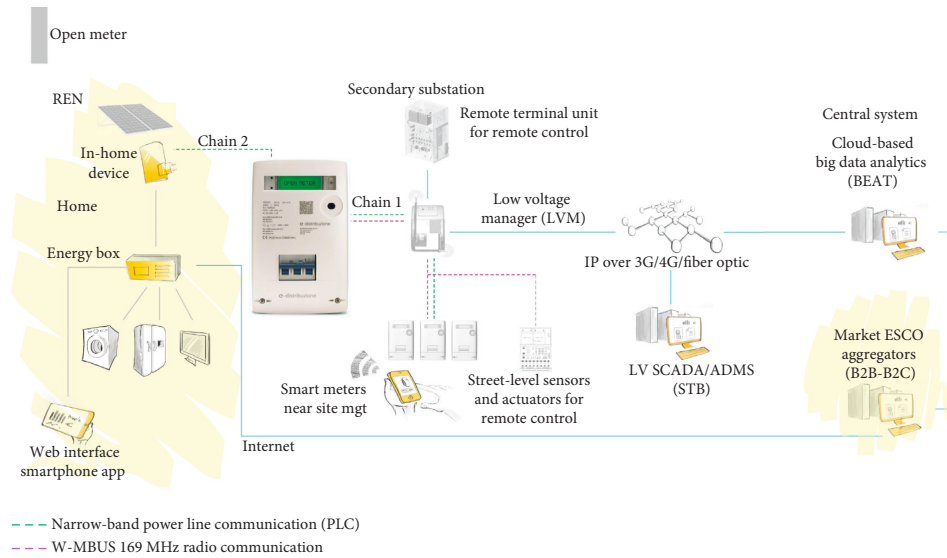


FIGURE 1: Telegestore system architecture.



FIGURE 2: Electrical energy meter 1G (a) and open energy meter 2G (b).

aware of how they use electricity, and can seize opportunities to achieve greater energy savings. Moreover, they represent a step towards the development of a smart grid [2–5].

Figure 3 reports the improved communication architecture with some more details. The new meters have two PLC channels: the first (chain 1) is devoted to the communication with the concentrator and the second for communication with in-house devices that could access to metering information through an open protocol (meters and more [6]). To enhance the reliability of the communication towards the concentrator, in addition to the main PLC channel, a radio module, with a transmission frequency at 169 MHz, is used as the backup channel. In fact, radio frequency (RF) communication should only be used when PLC fails, that is, in the case of particularly noisy wired communication (less than 5% of total) and obviously in case of disconnection of the power

line (e.g., blackout). The RF communication at 169 MHz is widely used in other applications in the wireless networks of sensors and/or meters (water, gas, electricity, and heat meters [7]). In the considered smart meters, it is applied for the first time in Italy for the electricity metering, and the studies summarized in this paper are aimed to assess the characteristics of the emission spectrum due to the 169 MHz radio module, by quantifying the total radiated power [8–11].

2. Mathematical Background

The total power radiated (TRP) by an electromagnetic source can be calculated by integrating the intensity of the radiation over the entire solid angle of 4π [8]. Considering the notations shown in Figure 4, it results

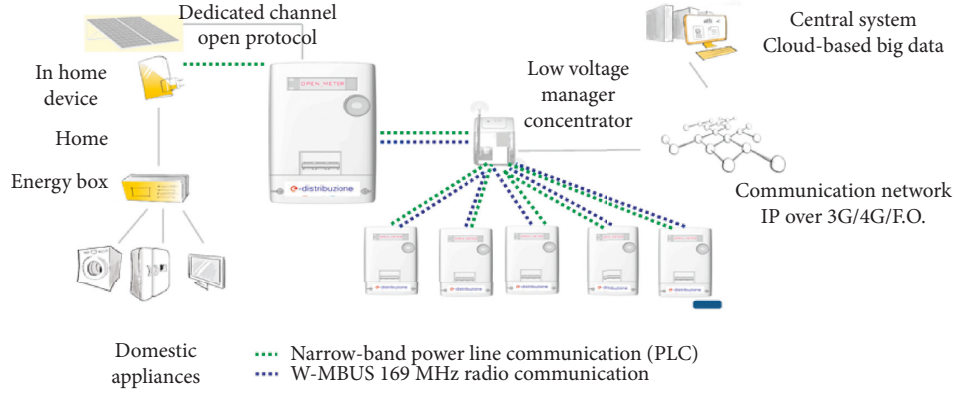


FIGURE 3: Open meter: the system architecture.

$$\text{TRP} = \iint_S R d\Omega = \int_0^{2\pi} \int_0^{\pi} R(\theta, \varphi) \cdot \sin(\theta) d\theta d\varphi, \quad (1)$$

where $d\Omega$ is the solid angle element equal to $\sin(\theta)d\theta d\varphi$.

It is also possible to define the equivalent isotropic radiated power (EIRP), which is a measure of power density that would be irradiated by an isotropic antenna with the same irradiated power:

$$\text{EIRP}(\theta, \varphi) = 4\pi \cdot R(\theta, \varphi), \quad (2)$$

from which

$$\text{TRP} = \frac{1}{4\pi} \int_0^{2\pi} \int_0^{\pi} \text{EIRP}(\theta, \varphi) \cdot \sin(\theta) d\theta d\varphi. \quad (3)$$

So, a quantification of the total radiated power can be obtained by measuring the EIRP in different positions.

Moreover, since the measurement must be taken in two polarizations, vertical and horizontal, it is possible to rewrite the equation based on the linear division of the terms of power with the polarization:

$$\text{TRP} = \frac{1}{4\pi} \int_0^{2\pi} \int_0^{\pi} (\text{EIRP}_{\theta}(\theta, \varphi) + \text{EiRP}_{\varphi}(\theta, \varphi)) \cdot \sin(\theta) d\theta d\varphi. \quad (4)$$

Finally, to calculate numerically the TRP from a set of measured values of the EIRP, it is necessary to perform a calculation of the integral by means of an approximation made by a discretization so that integral becomes a sum of values:

$$\text{TRP} \approx \frac{\pi}{2N \cdot M} \sum_{n=0}^{N-1} \sum_{m=0}^{M-1} (\text{EIRP}_{\theta}(\theta_n, \varphi_n) + \text{EIRP}_{\varphi}(\theta_n, \varphi_n)) \cdot \sin(\theta_n). \quad (5)$$

In equation (5), the sampled values of the EIRP, in N positions along the axis φ and in M positions along the axis θ , have to be inserted.

To take into account of the role of the transmitting and receiving antenna, it is possible to refer to the transmission

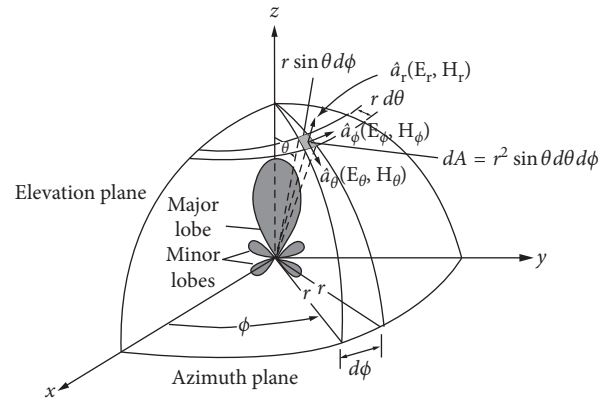


FIGURE 4: Spherical coordinate system for antenna analysis.

equation of Friis which binds the received and the transmitted power:

$$\frac{P_r}{\text{TRP}} = e_r e_t \frac{\lambda^2 D_r(\theta, \varphi) D_t(\theta, \varphi)}{(4\pi R)^2}, \quad (6)$$

where λ is the wavelength, e_t and e_r are the radiation efficiencies, A_t and A_r are the effective areas, and D_t and D_r are the directivities of transmitting and receiving antenna, respectively [8]. In reception, the antenna “transforms” the intensity of the incident electric field into voltage at its terminals that is then converted into power by the spectrum analyzer with a reference impedance of 50Ω . Therefore, to calculate the electric field value, it is necessary to introduce, as correction factor, a parameter that is called antenna correction or antenna factor (AF), and it depends on the frequency.

The definition of the antenna factor is

$$\text{AF} = \frac{E}{V}, \quad (7)$$

where E is the instantaneous intensity of the electric field incident on the antenna (V/m), V is the voltage value measured on the output connector of the same antenna (V), and AF is the antenna factor (m^{-1}).

We can rewrite equation (7) using the logarithmic amplitudes (dB) and introduce also P_{loss} that summarizes all

the losses of the measurement chain between the antenna and the instrument (for example, the loss of cables and other connection accessories):

$$E = V + AF + P_{\text{loss}} \quad (8)$$

3. Experimental Measurement Setup

3.1. Smart-Meter Configuration and Timing Measurements. The apparatus used in this paper for radiated performance testing was representative of the typical production units of the 2G meters, and it was configured to use the highest level of power in transmission on the RF channel. To speed up the measurement procedures, the firmware of the meter has been modified so that, as the device was supplied, it automatically and repetitively performs a normal transmission of metering data with a periodicity of about 2 s. This is not the normal use of the radio frequency channel, as already mentioned above, since the 2G meters use this transmission mode only occasionally (in case of disconnection) or in conditions of an anomalous operation of PLC. So, the normal transmission periodicity is too long to be compatible with repetitive measurements and has been reduced. No other changes have been made in the operation mode.

A preliminary laboratory characterization was done to measure the duration of the radio frequency emissions of a normal data transmission and to verify its periodicity. To this aim, a high-accuracy and high-frequency oscilloscope (LeCroy HDO4000 bandwidth 500 MHz, resolution 12-bit, sample rate up to 2.5 GHz) and a directive antenna (SmartAlaris DF-A0047 combined loop/log-periodic dipole array, frequency range 20–500 MHz) were used. During the tests, the 2G meter was fed through a normal electrical outlet and placed on a nonmetallic support base (wooden table). At the same height but at a distance of 3 m, in order to verify the far field conditions, the receiving antenna was placed and connected to the oscilloscope. The alignment and the distances were verified by means of a laser distance meter.

Specific software was implemented on the oscilloscope to perform the demodulation and the detection of the beginning and the ending of the 169 MHz transmission and to save the measured time intervals. With an acquisition time interval particularly long (20 s), it is possible to analyze both the duration of transmission and the time that elapses between two consecutive transmissions (Figure 5). The oscilloscope was left in acquisition for an hour to perform a statistical analysis. The average measured periodicity was 2.1 s with a variance of about 19% instead the average duration of transmission was 141 ms with a variance less than 1% (Figure 6).

3.2. Measurement Method for TRP. The measurement of the TRP from wireless devices is a well-established topic that was faced in numerous scientific papers [8–14] and in international standards [15], some of them even specifically focused on smart meters [16].

The alternative test procedures can significantly reduce the measurement time, but, of course, they lead to different

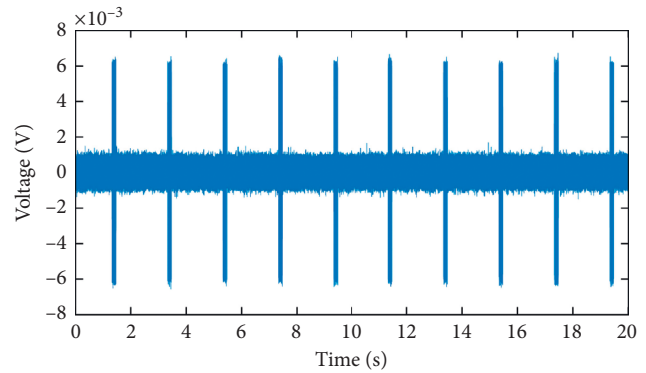


FIGURE 5: Example of a time-domain acquisition.

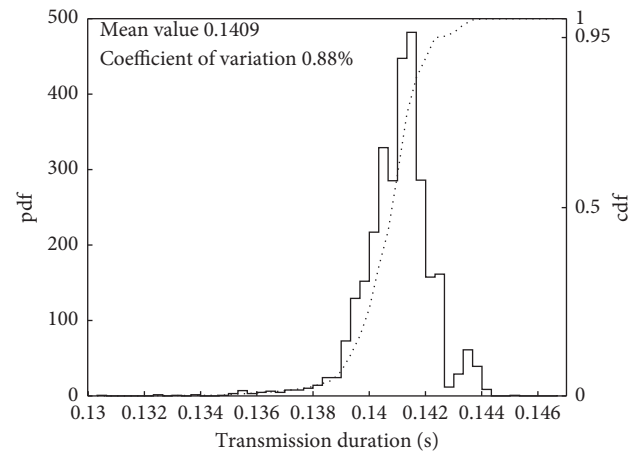


FIGURE 6: Statistical analysis of the transmission duration.

levels of measurement uncertainty in the obtained results. A comprehensive spherical spatial scan (Figure 7) could be particularly complex from the point of view of the implementation.

For the accuracy level aimed in this paper, a simplified procedure was preferred, and, mainly, the indications included in [16] were followed. The meter was located at a height of 1 m above the reference plane of a semianechoic room, on a 360° rotating table on the horizontal plane. Measurements were taken with discrete increments of 10° with receiving antenna configured for the horizontal polarizations; then all the angular configurations are repeated with the antenna configured for the vertical polarizations. The measurements were repeated over three planes for a total number of measurements equal to 216.

The measurements were carried out in accordance with the provisions of [17], and the TRP is the integral with respect to the spherical coordinates in agreement with equation (7).

3.3. Considerations on Uncertainty. In the execution of electromagnetic field measurements, there are several factors that must be considered for the calculation of uncertainty. In Table 1, there are a list of the main parameters and their typical characteristics of uncertainty that will be considered

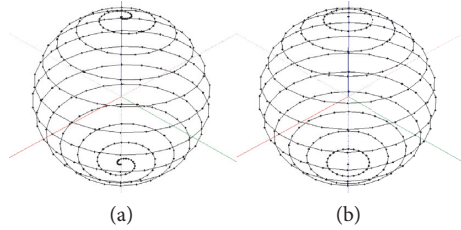


FIGURE 7: Spiral scan measurement points (a) and standard (equally spaced) measurement points (b).

in the following measurements. This leads to a typical combined uncertainty values of the order of 11% which corresponds to an expanded uncertainty ($k = 2$) of the order of 22%.

3.4. Semianechoic Room and Instrumentation. The characterization activities were carried out at the semianechoic chamber at the Electromagnetic Compatibility Laboratory of the Department of Electrical Engineering and Information “Maurizio Scarano” of the University of Cassino and Southern Lazio (Figure 8) whose dimensions are 9.1 m (length) \times 5.74 m (width) \times 6.24 m (height).

The semianechoic chamber is a normalized test environment shielded with respect to the external environment: the radiated emissions from the equipment under test are not influenced by the locally occurring background electromagnetic noise. In fact, the irradiated disturbances due to radiophonic, radio-television, and radio-mobile broadcasts can be eliminated or strongly attenuated by the shielding so that they do not disturb the immunity test that is carried. The RF shielding test provided the following values for attenuations:

- (i) Magnetic field 55 dB at 10 kHz, 90 dB at 100 kHz, and 100 dB at 1 MHz
- (ii) Electric field > 130 dB from 1 MHz to 1 GHz and 100 dB from 1 GHz to 18 GHz
- (iii) Planar wave > 130 dB from 1 MHz to 1 GHz and 100 dB from 1 GHz to 18 GHz

Moreover, the chamber walls are covered with ferrite tiles and cones with the ability to absorb electromagnetic waves to eliminate the reflected components and have uniformity in the relief mode. Since the floor is not equipped with fixed absorbent cones, the chamber is semianechoic and not fully anechoic.

Finally, the chamber is certified for tests and measurements at 3 meters, according to [18–22].

Outside the semianechoic chamber, there is a shielded control room in which the instrumentation used for the emission and immunity measurements are located (Figure 9).

All the operations, in fact, are piloted from the outside because the operators would become sources of disturbance.

The RF shielding test provided the following values for attenuations: 62 dB magnetic field at 10 kHz, 98 dB at 100 kHz, and 124 dB at 1 MHz; electric field > 131 dB from 1 MHz to 1 GHz and 147 dB from 1 GHz to 18 GHz; and

planar wave > 132 dB at 500 MHz, 130 dB at 1 GHz, 102 dB at 10 GHz, and 102 dB at 18 GHz.

The instrumentations used for the measurement are as follows: the broadband antenna, type HL-1000 (Figure 8) that is a combined antenna for EMC-measurement purposes composed by logarithmic-periodical and a biconical antenna (frequency range 20–1000 MHz; nominal impedance 50 Ω), and spectrum analyzer Rohde & Schwarz R&S FSH8-2005 (frequency range 100 kHz to 8 GHz; frequency resolution 1 Hz; absolute level uncertainty at 100 MHz < 0.3 dB) (Figure 10). The configuration used for the spectrum analyzer is reported in Table 2. All the used instruments are within the validity period of the calibration certificate.

The detected environmental conditions were as follows: temperature of 24 C and relative humidity of 48%.

In the illustrated condition at 169 MHz, the estimated uncertainty interval, considering a 95% level of confidence, was ± 4.2 dB.

3.5. Measurement Setup and Execution of Tests. For the tests, the 2G meter was placed on a nonmetallic support base (a wooden table). In order to verify the conditions of the far field, the receiving antenna was placed at the same height but at a distance of 3 m and then connected to the spectrum analyzer. Alignment and distances were verified by means of the laser distance meter.

The first evaluations were made with the insertion of ferrite cylinders on the supply line (Figure 11) to filter the electromagnetic emissions due to the power supply cables and then to determine the contribution due only to the 2G meter.

The antenna was configured for vertical polarization, the measurements of the radiated emissions were performed for enough time to stabilize the peak value, and the maximum level was recorded (max hold). The position of the 2G meter was rotated with an increase of 10° counterclockwise, and the measuring operations were repeated.

Position changes and measurements were repeated until a complete revolution was reached by returning the device to its initial position (36 measured values). The antenna was configured for horizontal polarization, and all position changes and measurements were repeated. All the described measurements were repeated over three different planes, [17].

4. Measurement Results

The obtained results in terms of emission diagrams are reported from Figures 12–17. The device comprehensively presents a good uniformity of emission. Considering the antenna factor and the cable attenuation, interpolating the measured values, and integrating numerically on the spherical surface (see equation (7)), the obtained total irradiated power was $TRP \approx 352$ mW, which corresponds to a value of average power density during transmission $W_0 \approx 3$ (mW/m²). Therefore, it results an intensity of average radiation during transmission $R \approx 27$ (mW/sr) and a maximum field strength $E \approx 0.6$ (V/m).

TABLE 1: Main uncertainty sources.

Uncertainty source	Absolute value (db)	Distribution	Coverage factor	Uncertainty (%)
Antenna factor, calibration	1.0	Norm.	2	5.0
Antenna factor, interpolation	1.0	Rect.	$\sqrt{3}$	5.8
Cable attenuation, calibration	0.2	Norm.	2	1.0
Impedance mismatch	1.0	Rect.	$\sqrt{3}$	5.8
Spectrum analyzer Accuracy	1.0	Rect.	$\sqrt{3}$	5.8



FIGURE 8: Test setup in the semianechoic room.

TABLE 2: Spectrum analyzer configuration.

Parameter	Setting
Trace	Max hold
Detect	RMS
Channel	BW: 10.00 kHz
Span	100 kHz
Center frequency	169.43 MHz
Trigger	Free run
RBW	300 Hz
VBW	3 MHz
Attenuation	40 dB
Measurement unit	dBm, dBuV



FIGURE 9: Instrumentations in the prechamber.

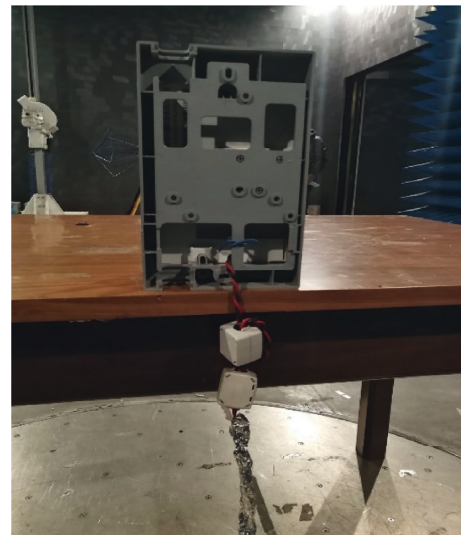


FIGURE 11: Location of the ferrites on the power cables.

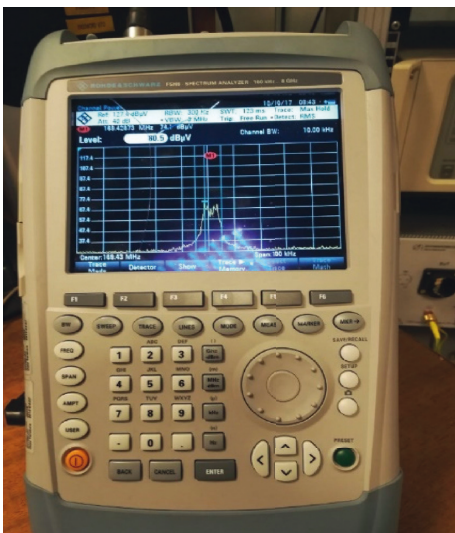


FIGURE 10: Spectrum analyzer FSH8.

In order to compare the measured emission levels with the limits of exposure to electromagnetic fields prescribed by the standards, the emission intensity should be measured and integrated over a certain time period. Referring to [23, 24], a 6 minutes time interval is here accounted. Moreover, as during normal operation, the time distance between transmissions is much higher than 6 minutes (typically 24 hours), and only one transmission was accounted to occur within this time interval. This implies that a duty cycle of 1/2500 is used for the calculation of the average values, obtaining $\bar{W} \approx 1.2 \mu\text{W}/\text{m}^2$ and $\bar{E} \approx 240 \mu\text{V}/\text{m}$. These values are much lower than the action level of 61 V/m for thermal effects (100 kHz to 300 GHz), reported in [23].

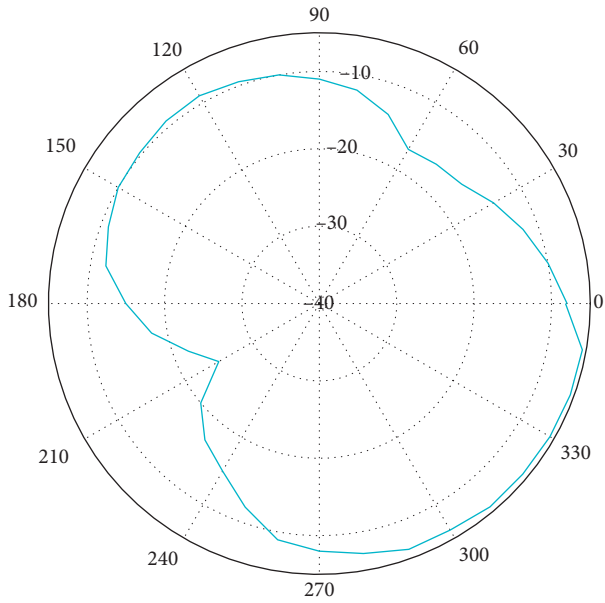


FIGURE 12: Emission diagram in horizontal polarization in the 1st plane (dbm).

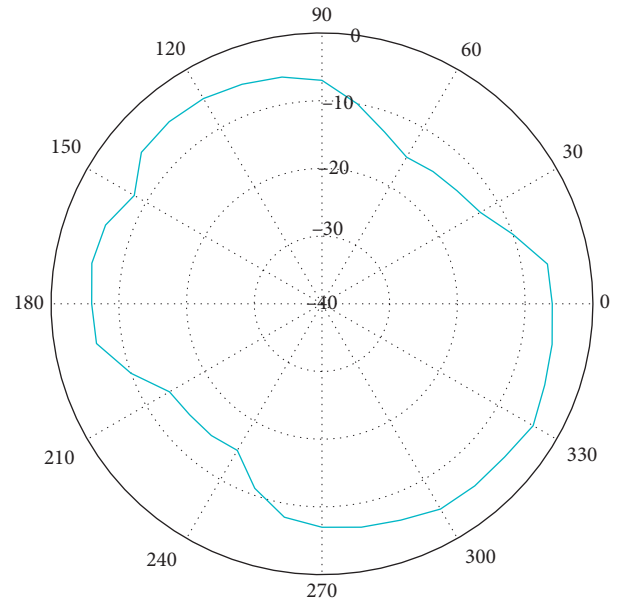


FIGURE 14: Emission diagram in horizontal polarization in the 3rd plane (dbm).

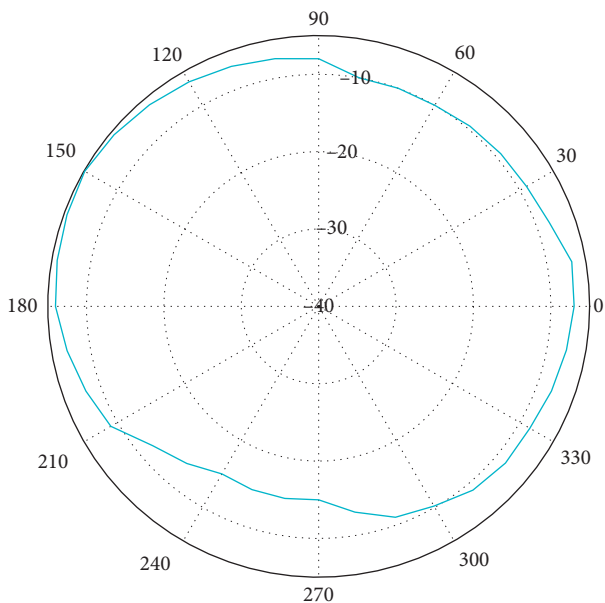


FIGURE 13: Emission diagram in horizontal polarization in the 2nd plane (dbm).

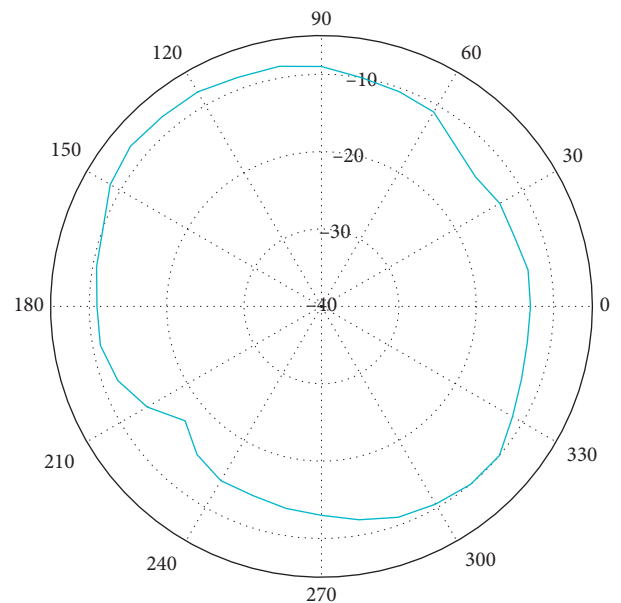


FIGURE 15: Emission diagram in vertical polarization in the 1st plane (dbm).

The measurements were repeated without the ferrite filters obtaining a remarkable increment in the measured values as reported in Table 3. Nevertheless, also in this case, the values are enormously lower than the action level.

The final activities had the purpose to verify whether the power values emitted by the RF transmission module significantly change during the normal operation of the 2G meter, e.g., during the supply of active or reactive energy.

For these activities, an environment similar to that of normal installation was considered (Measurement Laboratory

at Engineering Department of the University of Campania “Luigi Vanvitelli,” Figure 18) [25–28].

To the described aim, the 2G meter was fed through the calibrator (Fluke Calibration 6105 A/50 A) to obtain a controlled power supply both in terms of amplitude and of power factor. At the same height but at a distance of 3 m in order to verify the far field conditions, the receiving antenna (SmartAlaris DF-A0047) was placed and connected to the spectrum analyzer RSA5106B (real-time spectrum analyzer, 17 dBm 3rd-order intercept at 2 GHz, ± 0.3 dB absolute

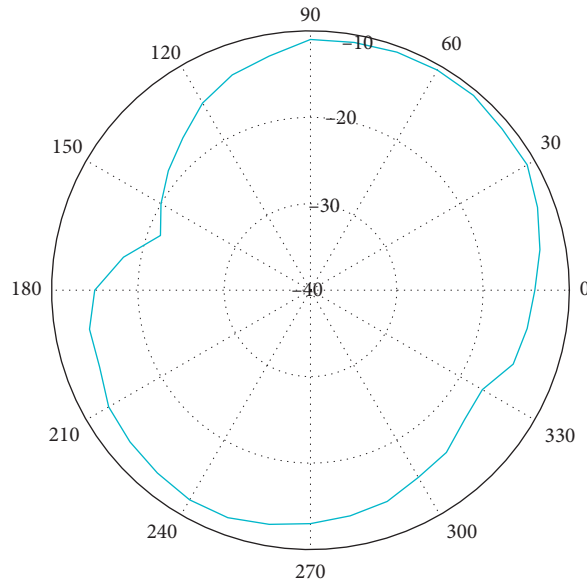
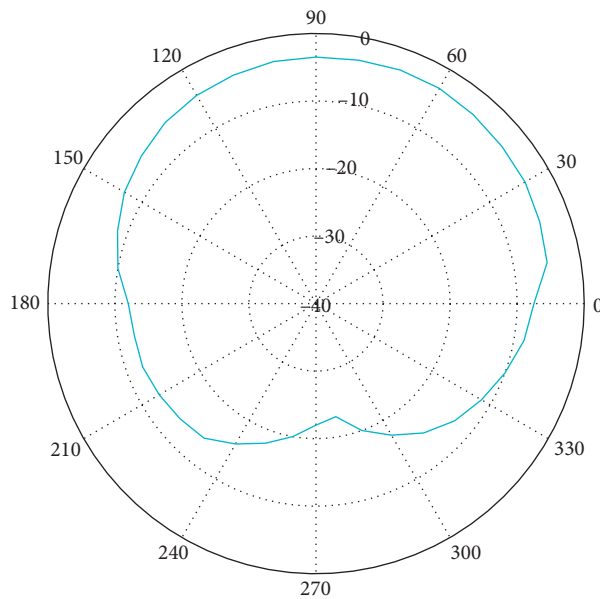
FIGURE 16: Emission diagram in vertical polarization in the 2nd plane (dbm).FIGURE 17: Emission diagram in vertical polarization in the 3rd plane (dbm).

TABLE 3: Measurement results.

Ferrite	TRP (mW)	W_0 (mW/m ²)	R (mW/sr)	E (V/m)	\bar{W} (μ W/m ²)	\bar{E} (μ V/m)
Yes	352	3	27	0.6	1.2	240
No	690	6	56	0.9	2.4	360

amplitude accuracy to 3 GHz, and real-time spurious free dynamic range of 80 dB). Alignment and distances have been verified by means of a laser distance meter. All the measurement operations were carried out with ferrites inserted on the power supply line, in order to filter the electromagnetic emissions due to the power supply cables and to measure the effect of the 2G meter only. At first, a reference emission level was measured without current

flowing. The current level was increased in 10% steps up to 100% of the nominal value with a power factor equal to 1, thus measuring only the active energy. Deviations in the level of emission were recorded. The operations were repeated with power factor 0.7, so determining the flowing of active and reactive energy at the same time. No significant changes in the emission levels were recorded within accuracy limits.



FIGURE 18: Measurements in normal installation condition.

5. Conclusion

This paper describes the characteristics of the emission at 169 MHz due to the RF module used as a backup channel of the Enel Open Meter 2G, by quantifying the total radiated power. The analyses were performed in an anechoic room, to obtain repeatable results, but also in situations close to normal operating conditions. On the basis of the measurement results, the intensity of the emitted field and the power density associated with the transmission of data are far lower than all the regulatory limits, both in peak values during transmission and even more in average values, being in both cases completely irrelevant in terms of electromagnetic pollution. Even if the coupling of the cables can produce positive interactions, which amplifies the values up to determine the doubling of the emission intensity values, the measured levels remain totally negligible. Moreover, no significant deviation was found in the emission pattern in conditions comparable to normal operating conditions.

Data Availability

The data are available upon request to the authors.

Conflicts of Interest

The authors declare that they have no conflicts of interest.

References

- [1] B. Botte, V. Cannatelli, and S. Rogai, "The telegestore project in Enel's metering system," in *Proceedings of the CIRED 2005—18th International Conference and Exhibition on Electricity Distribution*, IET Turin, Italy, June 2005.
- [2] A. Delle Femine, D. Gallo, D. Giordano, C. Landi, M. Luiso, and D. Signorino, "Synchronized measurement system for railway application," *Journal of Physics: Conference Series*, vol. 1065, no. 5, Article ID 052040, 2018.
- [3] A. Cataliotti, V. Cosentino, G. Crotti et al., "Compensation of nonlinearity of voltage and current instrument transformers," in *IEEE Transactions on Instrumentation and Measurement*, vol. 68, no. 5, pp. 1322–1332, 2019.
- [4] A. J. Collin, A. Delle Femine, D. Gallo, R. Langella, and M. Luiso, "Compensation of current transformers' nonlinearities by means of frequency coupling matrices," in *Proceedings of the 2018 IEEE 9th International Workshop on Applied Measurements for Power Systems (AMPS)*, pp. 1–6, IEEE, Bologna, Italy, September 2018.
- [5] G. Crotti, A. Delle Femine, D. Gallo et al., "Calibration of current transformers in distorted conditions," *Journal of Physics: Conference Series*, vol. 1065, no. 5, Article ID 052033, 2018.
- [6] <http://www.metersandmore.com/>.
- [7] M. Barbiroli, F. Fuschini, G. Tartarini, and G. E. Corazza, "Smart metering wireless networks at 169 MHz," *IEEE Access*, vol. 5, pp. 8357–8368, 2017.
- [8] C. A. Balanis, *Antenna Theory - Analysis and Design*, ISBN 0-471-66782-X, John Wiley & Sons, Inc., Hoboken, NJ, USA, 2005.
- [9] H. Garbe and S. Battermann, "Converting total-radiated-power measurements to equivalent E-field data," in *Proceedings of the 2008 IEEE International Symposium on Electromagnetic Compatibility*, pp. 1–6, IEEE, Detroit, MI, USA, August 2008.
- [10] H. G. Krauthausser and J. Nitsch, "Simplifying the measurement of total radiated power in reverberation chambers," in *Proceedings of the 2007 International Conference on Electromagnetics in Advanced Applications*, pp. 768–771, IEEE, Torino, Italy, September 2007.
- [11] J. Krogerus, K. Kiesi, and V. Santomaa, "Evaluation of three methods for measuring total radiated power of handset antennas," in *Proceedings of the 18th IEEE Instrumentation and Measurement Technology Conference*, vol. 2, pp. 1005–1010, IEEE, Budapest, Hungary, May 2001.
- [12] H. Arai, "Sampling points reduction in spherical scanned TRP measurement," in *Proceedings of the 2014 IEEE Conference on Antenna Measurements & Applications*, pp. 1–4, IEEE, Antibes Juan-les-Pins, France, November 2014.
- [13] O. M. Bucci, C. Gennarelli, and C. Savarese, "Optimal interpolation of radiated fields over a sphere," *IEEE Transactions on Antennas and Propagation*, vol. 39, no. 11, pp. 1633–1643, 1991.
- [14] O. M. Bucci, F. D'Agostino, C. Gennarelli, G. Riccio, and C. Savarese, "Data reduction in the Nf-Ff transformation technique with spherical scanning," *Journal of Electromagnetic Waves and Applications*, vol. 15, no. 6, pp. 755–775, 2001.
- [15] CTIA Certification, *Test Plan for Mobile Station Over the Air Performance—Method of Measurement for Radiated RF Power and Receiver Performance, Rev. 3.7.1*, CTIA-The Wireless Association, Washington, DC, USA, 2018.
- [16] UNI/TS 11291-11-4:2014, *Gas Measurement Systems—Hourly Based Gas Metering Systems—Part 11-4: Communication Profile Pm1 Italian Standards*, Ente Nazionale Italiano di Unificazione, Milan, Italy, 2014.
- [17] ETSI EN 300-220-1: 2012, *Electromagnetic Compatibility and Radio Spectrum Matters (ERM); Short Range Devices (SRD); Radio Equipment to Be Used in the 25 MHz to 1000 MHz Frequency Range with Power Levels Ranging up to 500 mW; Part 1: Technical Characteristics and Test Methods*, South African Bureau of Standards, Pretoria, South Africa, 2012.
- [18] CENELEC-EN 50147-1: 1996, *Anechoic Chambers Part 1: Shield Attenuation Measurement*, European Committee for Electrotechnical Standardization, Brussels, Belgium, 1996.
- [19] IEC 61326-3-1:2017, *Released for Electrical Equipment for Measurement, Control and Laboratory Use—EMC Requirements*, International Electrotechnical Commission, Geneva, Switzerland, 2017.

- [20] CENELEC EN 55022 2014 + Am.1: 2018, *Information Technology Equipment—Radio Disturbance Characteristics—Limits and Methods of Measurement*, European Committee for Electrotechnical Standardization, Brussels, Belgium, 2018.
- [21] G. Betta, D. Capriglione, L. Ferrigno, and M. Laracca, “A measurement driven approach to design an efficient test methodology for PLT network QoS performance parameters assessment,” *Measurement Science Technology*, vol. 20, no. 5, 2009.
- [22] G. Betta, D. Capriglione, L. Ferrigno, and G. Miele, “Influence of Wi-Fi computer interfaces on measurement apparatuses,” *IEEE Transactions on Instrumentation and Measurement*, vol. 59, no. 12, pp. 3244–3252, 2010.
- [23] European Agency for Safety and Health at Work, *Directive 2013/35/EU-Electromagnetic Fields*, European Agency for Safety and Health at Work, Bilbao, Spain, 2013.
- [24] European Agency for Safety and Health at Work, *Non-binding Guide to Good Practice for Implementing Directive 2013/35/EU Electromagnetic Fields, Guide for SMEs*, European Agency for Safety and Health at Work, Bilbao, Spain, 2013.
- [25] S. Del Prete, A. Delle Femine, D. Gallo, C. Landi, and M. Luiso, “Implementation of a distributed stand alone merging unit,” *Journal of Physics: Conference Series*, vol. 1065, no. 5, Article ID 052042, 2018.
- [26] G. Crotti, A. D. Femine, D. Gallo, D. Giordano, C. Landi, and M. Luiso, “Measurement of the absolute phase error of digitizers,” in *IEEE Transactions on Instrumentation and Measurement*, vol. 68, no. 6, pp. 1724–1731, 2019.
- [27] G. Crotti, D. Giordano, P. Roccato et al., “Pantograph-to-OHL arc: conducted effects in DC railway supply system,” in *Proceedings of the 2018 IEEE 9th International Workshop on Applied Measurements for Power Systems (AMPS)*, pp. 1–6, IEEE, Bologna, Italy, September 2018.
- [28] G. Crotti, D. Giordano, A. Delle Ferninc, D. Gallo, C. Landi, and M. Luiso, “A testbed for static and dynamic characterization of DC voltage and current transducers,” in *Proceedings of the 2018 IEEE 9th International Workshop on Applied Measurements for Power Systems (AMPS)*, pp. 1–6, Bologna, Italy, September 2018.



Hindawi

Submit your manuscripts at
www.hindawi.com

